

Electronic Supplementary Information (ESI) for:

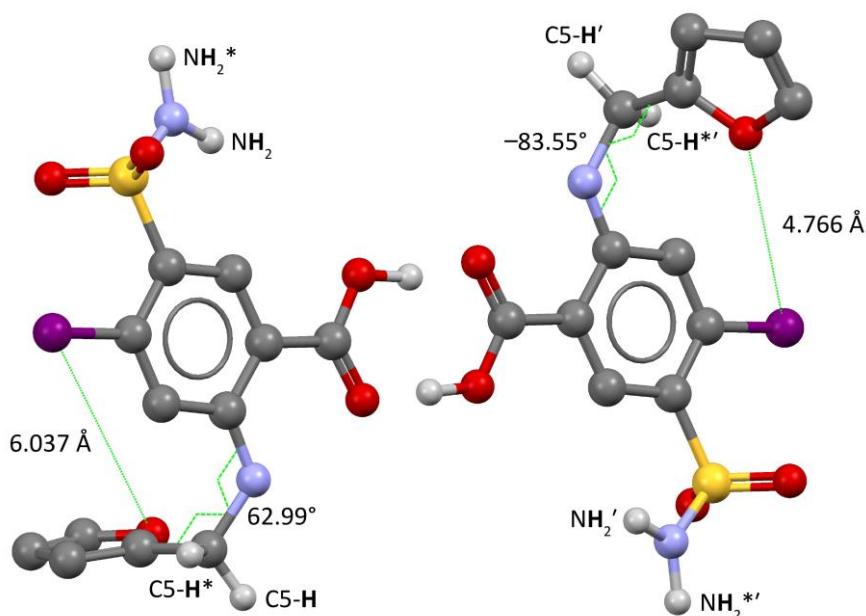
Furosemide's One Little Hydrogen Atom: NMR Crystallography Structure Verification of Powdered Molecular Organics

Cory M. Widdifield, Harry Robson and Paul Hodgkinson*

Department of Chemistry, University of Durham, Durham DH1 3LE, UK

Table of Contents

Scheme S1. Specification of Naming Convention for Molecules in the Asymmetric Unit of Furosemide	S2
Table S1. Experimental SSNMR Details	S3
Table S2. Experimentally measured ¹³ C chemical shifts – S-A sample	S4
Table S3. Experimentally measured ¹ H chemical shifts – S-A sample	S4
Figure S1. Powder X-ray patterns for furosemide (FURSEM01/FURSEM17/S-A)	S5
Figure S2. Simulated powder X-ray diffraction patterns for furosemide (scaled, for FURSEM01/FURSEM17)	S5
Table S4. Crystal data and structure refinement for FURSEM-NEW	S6
Figure S3. ¹³ C SSNMR spectra comparing CP/MAS vs. direct excitation for S-A sample of furosemide	S7
Figure S4. ¹³ C CP/MAS NMR spectra for ReCryst and S-A	S7
Figure S5. ¹⁵ N CP/MAS NMR spectrum of the S-A sample of furosemide	S8
Figure S6. ¹ H fast MAS NMR spectra of furosemide (S-A and ReCryst samples)	S8
Figure S7. $T_1(^1\text{H})$ measurement for the S-A sample of furosemide	S9
Figure S8. Partial expanded view of ¹ H- ¹³ C FSLG-HETCOR NMR spectra with site assignments for S-A sample	S10
Figure S9. Partial expanded view of ¹ H- ¹³ C FSLG-HETCOR NMR spectra with site assignments for S-A sample	S10
Table S5. Computational details and computed system enthalpies	S11
Table S6. GIPAW DFT-computed magnetic shielding values for various furosemide crystal structures	S12
Figure S10. Correlation plots relating ¹ H isotropic magnetic shielding with experimental isotropic chemical shifts	S13
Figure S11. Correlation plots relating ¹³ C isotropic magnetic shielding with experimental isotropic chemical shifts	S14
Figure S12. Correlation plots relating computed ¹ H isotropic chemical shift value changes and lattice enthalpy changes with OH internuclear distance variation	S15
Figure S13. Comparison between calculated and experimental SSNMR for ¹³ C (FURSEM01/FURSEM17/S-A)	S15
Table S7. ¹ H RMSD calculation for FURSEM-NEW (H-opt)	S16
References	S17



Scheme S1. Naming Convention for Molecules in the Asymmetric Unit of Furosemide. As denoted in the main text, we have arbitrarily labelled atomic sites in one of the two furosemide molecules in the asymmetric unit with primes ('). This is the molecule (on right) having a $\text{C}_{\text{ring}}\text{-NH-CH}_2\text{-C}_{\text{furan}}$ torsion angle (absolute value) of approximately $80 - 85^\circ$ (across all **FURSEM01**, **FURSEM17**, and **FURSEM-NEW** structures). This is also the furosemide molecule where the oxygen atom of the furan ring is significantly closer to the chlorine of the benzene ring. Additionally, we note that our labels are such that C5-H/C5-H' have torsion angles (i.e., $\text{C}_{\text{ring}}\text{-NH-C-H}$, abs. value) with the benzene ring that are significantly more than 90° (approaching 180°), while C5-H*/C5-H*' have torsion angles (abs. value) with the benzene that are less than 90° . Likewise, before geometry optimisations in **FURSEM01** and **FURSEM17**, the $\text{NH}_2^*/\text{NH}_2^{*'}$ have torsion angles (abs. value) with the benzene ring approaching 180° , while NH_2/NH_2' have torsion angles (abs. value) with the benzene ring nearing 0° . After geometry optimisations for **FURSEM01** and **FURSEM17**, and in all calculations upon **FURSEM-NEW**, the orientations of the optimised NH_2 group hydrogen atoms are such that this method of distinction is no longer adequate, and in these cases, NH_2/NH_2' have torsion angles with the furan ring (i.e., $\text{C}_{\text{ring}}\text{-CH}_2\text{-N-H}$, abs. value) of much less than 90° , while $\text{NH}_2^*/\text{NH}_2^{*'}$ have torsion angles with the furan ring (abs. value) of much greater than 90° .

Table S1. Experimental SSNMR Details^a

nuclide(s)	window / kHz (f_2, f_1)	points (t_2, t_1)	$\pi/2$ / μs	scans	recycle delay / s	contact time / μs	MAS frequency / kHz ^b	τ_1, τ_2 / μs	details
¹³ C	50.00	4994	2.5	88	50.0	3000	12.50	—	S-A sample. 4 mm MAS probe; cross-polarization (CP)/MAS experiment; ramped CP; $T = 298$ K.
¹³ C, ¹ H	25.00, 26.48	1746, 64	2.5	48	50.0	100	13.24	—	S-A sample. 4 mm MAS probe; refocused frequency-switched Lee-Goldberg (FSLG)-HETCOR experiment; ramped CP; $T = 293 \pm 1$ K; carbon-13 π pulse = 8.4 μs .
¹³ C	50.00	4994	4.1	16384	2.0	—	13.50	67.9, 20.0	S-A sample. 4 mm MAS probe; Hahn echo experiment; $T = 293 \pm 1$ K.
¹³ C, ¹ H	25.00, 26.48	1746, 70	2.5	16	50.0	300	13.50	—	S-A sample. 4mm MAS probe; refocused FSLG-HETCOR experiment; ramped CP; $T = 294 \pm 1$ K; carbon-13 π pulse = 8.4 μs
¹³ C	50.00	4994	2.5	896	60.0	2500	13.5 (unreg.)	—	ReCryst sample. 1.3 mm MAS probe; CP/MAS experiment; $T = 293 \pm 2$ K; co-added with data below to arrive at spectrum in Figure S4a.
¹³ C	50.00	4994	2.5	3920	30.0	2500	13.5 (unreg.)	—	ReCryst sample. 1.3 mm MAS probe; CP/MAS experiment; $T = 293 \pm 2$ K.
¹ H	100.00	1244	3.2	16	50.0	—	60.3 (unreg.)	—	S-A sample. 1.3 mm MAS probe; Bloch decay; $T = 273 \pm 2$ K to ensure sample temperature of ca. 298 K (compensate for frictional heating due to fast MAS).
¹ H	100.00	988	2.5	4	varied	—	12.50	—	S-A sample. 4 mm MAS probe; T_1 measurement.
¹ H	41.67	1244	2.5	16	50.0	—	60.00	—	ReCryst sample. 1.3 mm MAS probe; Bloch decay; $T = 273 \pm 2$ K to compensate for heating.
¹ H	100.00	988	2.5	4	varied	—	13.5 (unreg.)	—	ReCryst sample. 1.3 mm MAS probe; T_1 measurement; $T = 273 \pm 2$ K.
¹⁵ N	50.00	2994	3.3	4096	50.0	5000	10.00	—	S-A sample. 4 mm MAS probe; CP/MAS experiment; $T = 293 \pm 1$ K; referenced against glycine ($\delta_{\text{iso}} = -347.58$ ppm); a series of 8 spectra were co-added to produce final spectrum.

^a SSNMR experiments were performed using an Oxford superconducting magnet operating at 11.7 T, and a Bruker AVANCE IIIHD console. This corresponds to ¹H, ¹³C and ¹⁵N Larmor frequencies of approximately 499.69, 125.65, and 50.65 MHz, respectively. All ¹H and ¹³C chemical shifts were referenced using adamantane ($\delta_{\text{iso}}(^1\text{H}) = 1.87$ ppm; $\delta_{\text{iso}}(^{13}\text{C}) = 38.48$ ppm) in the usual manner. All ¹³C experiments used SPINAL64 heteronuclear decoupling during acquisition. Prior to NMR experiments, samples were lightly ground for a few minutes to ensure a fine powder. It has been previously established that polymorphic forms of furosemide will interconvert to the 'form 1' polymorph, but this requires ca. 1 – 2 hours of vigorous sample grinding.¹

^b Unless otherwise denoted, the MAS frequency was regulated to ± 3 Hz for the 4 mm MAS probe, and ± 10 Hz for the 1.3 mm MAS probe.

Table S2. Experimentally measured ^{13}C chemical shifts – **S-A** sample^a

Assignment	$\delta_{\text{iso}} / \text{ppm}$	Assignment	$\delta_{\text{iso}} / \text{ppm}$
12	172.25	9	ca. 127.1(0.2) ^c
6	ca. 155.2(0.3) ^b	9'	ca. 125.2(0.2) ^c
6	ca. 154.0(0.3) ^b	7	ca. 117.1(0.2) ^c
4'	153.51	7'	ca. 116.8(0.2) ^c
4	150.60	2'	112.09
1	144.23	2 / 3	110.53
1'	141.54	3'	109.37
8	ca. 138(2) ^c	11	108.61
10'	136.60	11'	106.06
10	135.36	5 / 5'	ca. 39.6(0.1) ^b

^a Equivalent shifts were measured on the re-crystallized sample. Measurement precision is estimated to be ± 0.05 ppm, unless otherwise stated in parentheses.

^b Coupling to ^{14}N is evident due to residual dipolar coupling (RDC) under MAS.

^c Coupling to $^{35/37}\text{Cl}$ nuclei is evident due to RDC.

Table S3. Experimentally Measured ^1H Chemical Shifts – **S-A** sample^a

Assignment	$\delta_{\text{iso}} / \text{ppm}$	Assignment	$\delta_{\text{iso}} / \text{ppm}$
OH / OH'	12.7	NH₂' (avg.)	6.5(0.2)
10'	8.7	2'	6.4
10	8.6	7	6.2
NH / NH'	8.4(0.2)	2 / 3	6.0
7'	7.9	3'	5.7
1	7.7	5*'	5.6
NH₂ (avg.)	6.7(0.2)	5 (avg.)	4.3
1'	6.5	5'	3.8

^a Measurement precision is estimated to be ± 0.1 ppm, unless otherwise stated in parentheses. The asterisk notation (*) serves to distinguish between the two chemically inequivalent hydrogen atoms in the CH_2 group of furosemide, as specified in more detail in Scheme S1.

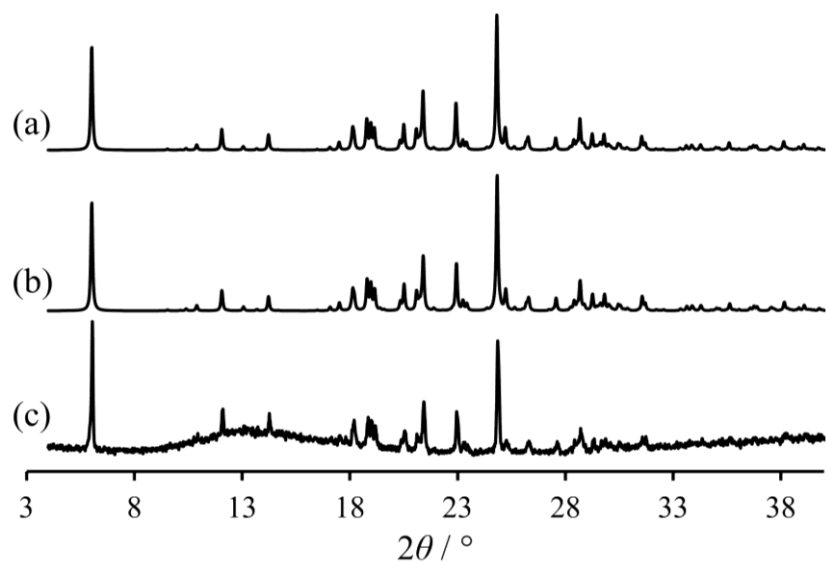


Figure S1. Powder X-ray patterns for furosemide. (a) and (b) correspond to simulated pXRD patterns using the crystal structures specified by **FURSEM17** and **FURSEM01**, respectively. (c) corresponds to experimental data acquired on the **S-A** sample of furosemide using a Bruker D8000 at room temperature with a Cu-K α 1 source ($\lambda = 1.5406 \text{ \AA}$).

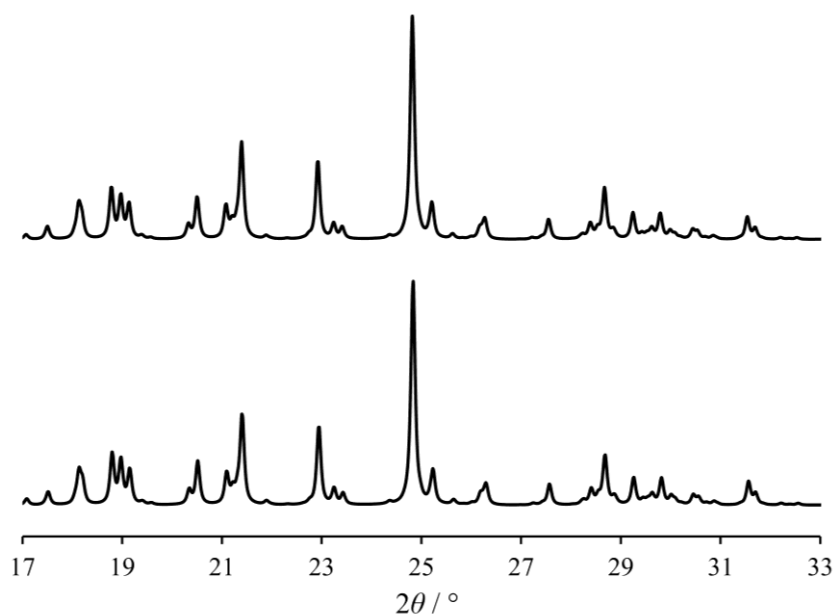


Figure S2. Simulated powder X-ray diffraction patterns for furosemide, scaled to better show fine details and highlight the high level of similarity in the simulated patterns corresponding to **FURSEM17** (top) and **FURSEM01** (bottom). All else has been maintained as in traces (a) and (b) of Figure S1.

Table S4. Crystal data and structure refinement for **FURSEM-NEW**^a

Empirical formula	C ₁₂ H ₁₁ ClN ₂ O ₅ S
Formula weight / amu	330.74
Temperature / K	120.0(2)
Crystal system	triclinic
Space group	P-1
<i>a</i> / Å	9.5347(5)
<i>b</i> / Å	10.4694(6)
<i>c</i> / Å	15.6057(9)
α / °	92.938(5)
β / °	107.085(5)
γ / °	116.622(6)
Volume / Å ³	1300.35(13)
Z	4
ρ_{calc} / g/cm ³	1.689
μ / mm ⁻¹	0.479
F(000)	680.0
Crystal size / mm ³	0.28 × 0.13 × 0.04
Radiation	MoK α (λ = 0.71073 Å)
2 θ range for data collection / °	4.46 to 58
Index ranges	-12 ≤ <i>h</i> ≤ 12, -14 ≤ <i>k</i> ≤ 14, -21 ≤ <i>l</i> ≤ 21
Reflections collected	19564
Independent reflections	6913 [<i>R</i> _{int} = 0.0797, <i>R</i> _{sigma} = 0.1153]
Data/restraints/parameters	6913/43/467
Goodness-of-fit on <i>F</i> ²	0.994
Final <i>R</i> indexes [<i>I</i> ≥ 2 σ (<i>I</i>)]	<i>R</i> ₁ = 0.0561, <i>wR</i> ₂ = 0.0935
Final <i>R</i> indexes [all data]	<i>R</i> ₁ = 0.1193, <i>wR</i> ₂ = 0.1209
Largest diff. peak/hole / e Å ⁻³	0.51/-0.66

^a CCDC deposition number: 1458460. Diffraction data were collected using an Agilent XCalibur (Sapphire-3 CCD detector, fine-focus sealed tube, graphite monochromator) diffractometer equipped with a Cryostream (Oxford Cryosystems) open-flow nitrogen cryostat. The structure was solved by direct methods and refined by performing a full-matrix least squares fit on *F*² for all data using Olex2² and SHELXTL³ software. Hydrogen atoms were found in the residual Fourier map and refined freely with an isotropic ADP.

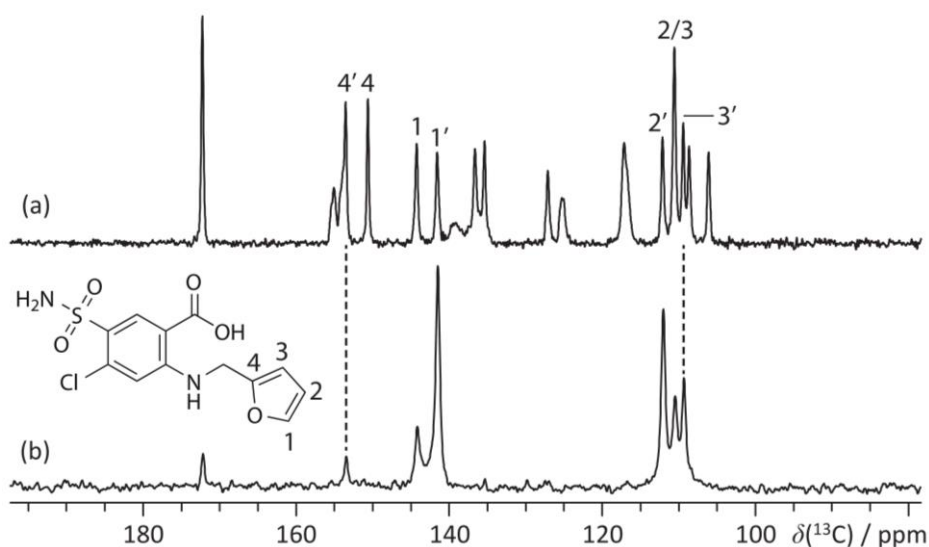


Figure S3. ^{13}C SSNMR spectra comparing CP/MAS (a) vs. direct excitation (Hahn echo) (b) for the **S-A** sample of furosemide at $B_0 = 11.7\text{ T}$ ($\nu_{\text{MAS}} = 13.50\text{ kHz}$, $T = 293\text{ K}$). As the direct excitation spectrum was acquired with a short recycle delay of 2.0 s, it is clear that the furan rings of each furosemide molecule in the asymmetric unit are dynamic with a timescale for the motion similar to the inverse of the ^{13}C Larmor frequency (ca. 10 ns). The dynamics of each ring appear to be slightly different, allowing us to distinguish them and provide an assignment.

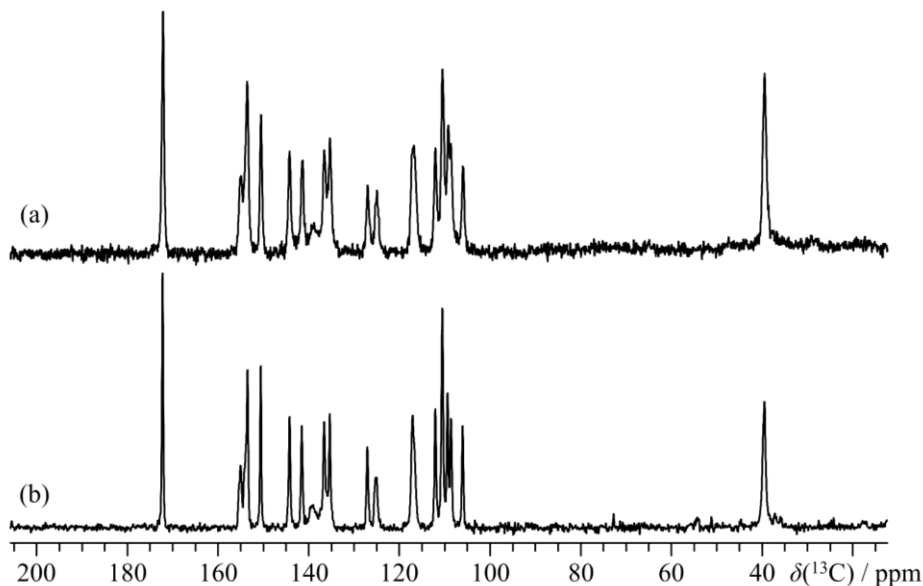


Figure S4. ^{13}C CP/MAS NMR spectra at $B_0 = 11.7\text{ T}$ for **ReCryst** (a) and **S-A** (b) samples of furosemide. Due to the limited amount of sample available for **ReCryst**, we performed the experiment in a 1.3 mm (o.d.) MAS rotor, while the **S-A** sample experiment was carried out in a 4.0 mm rotor. In (a), $\nu_{\text{MAS}} = 13.5(1)\text{ kHz}$, 4 816 transients were averaged with a recycle delay of 30 – 60 s and $T = 293\text{ K}$. In (b), $\nu_{\text{MAS}} = 12.50\text{ kHz}$, 88 transients were averaged with a recycle delay of 50 s and $T = 298\text{ K}$ (see Table S1 for details).

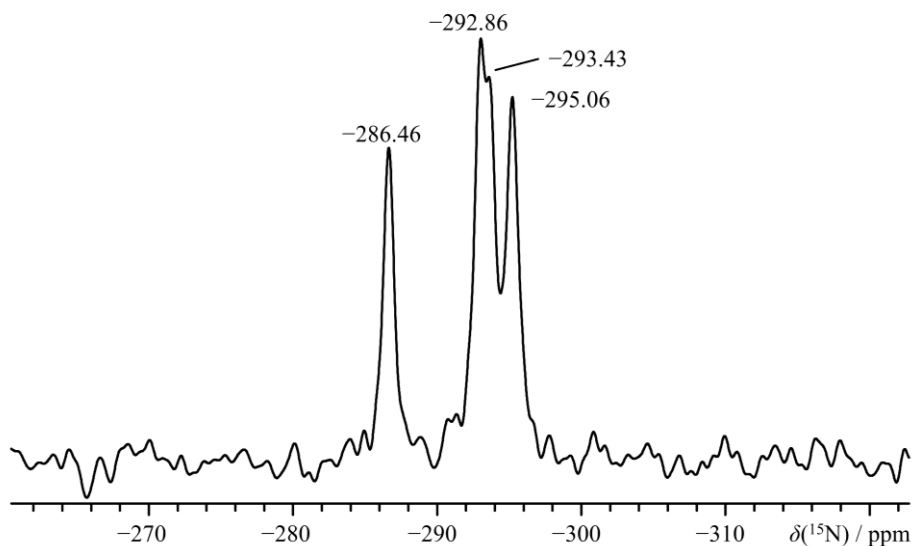


Figure S5. ^{15}N CP/MAS NMR spectrum of the **S-A** sample of furosemide, acquired at $B_0 = 11.7$ T and $\nu_{\text{MAS}} = 10$ kHz. Spectrum is the result of collecting 4 096 transients (cross-polarization contact time of 5 ms), with a recycle delay of 50 s. Chemical shifts of observed peaks are indicated, and were measured to within ± 0.05 ppm.

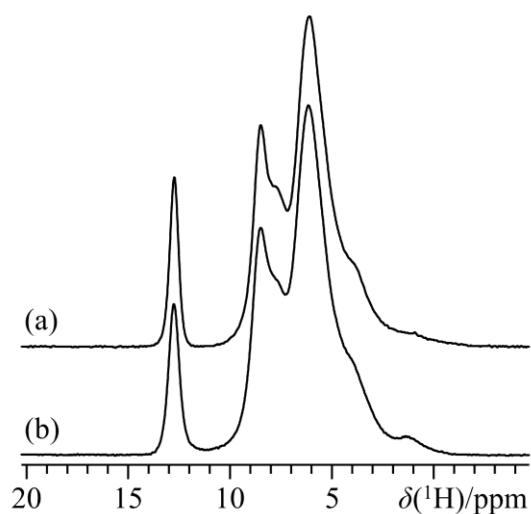


Figure S6. ^1H fast MAS NMR spectra of furosemide at $B_0 = 11.7$ T, both from the **S-A** sample (a), and from the **ReCryst** sample used to determine the crystal structure **FURSEM-NEW** in the present report (b). In (a), 16 transients were collected at $\nu_{\text{MAS}} = 60.3$ kHz, while in (b), 8 transients were collected at $\nu_{\text{MAS}} = 60.00$ kHz. In both, the recycle delay was 50 s. The temperature was corrected to account for the frictional heating under fast MAS via K^{79}Br using the method of Thurber and Tycko,⁴ and is such that the temperature *at the sample* was approximately 298 K.

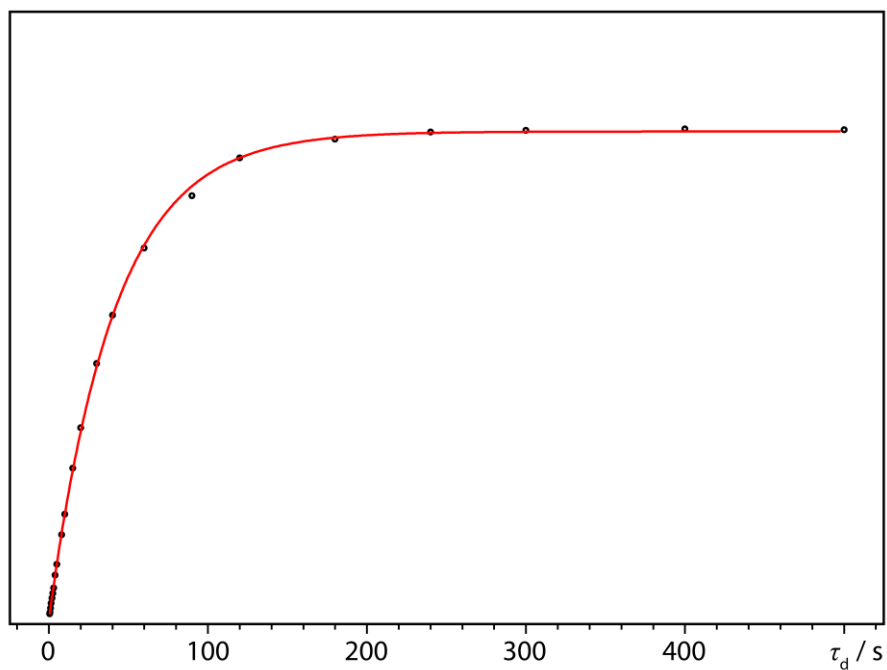


Figure S7. $T_1(^1\text{H})$ measurement for the **S-A** sample of furosemide, acquired using the saturation recovery pulse sequence at $B_0 = 11.7$ T, $\nu_{\text{MAS}} = 12.50$ kHz, and ambient temperature. The data (black circles) were fit to an exponential recovery function (red) and yielded a T_1 of ca. 41 s. A similar measurement for the **ReCryst** sample of furosemide (not shown) also furnished a T_1 of ca. 41 s under similar conditions.

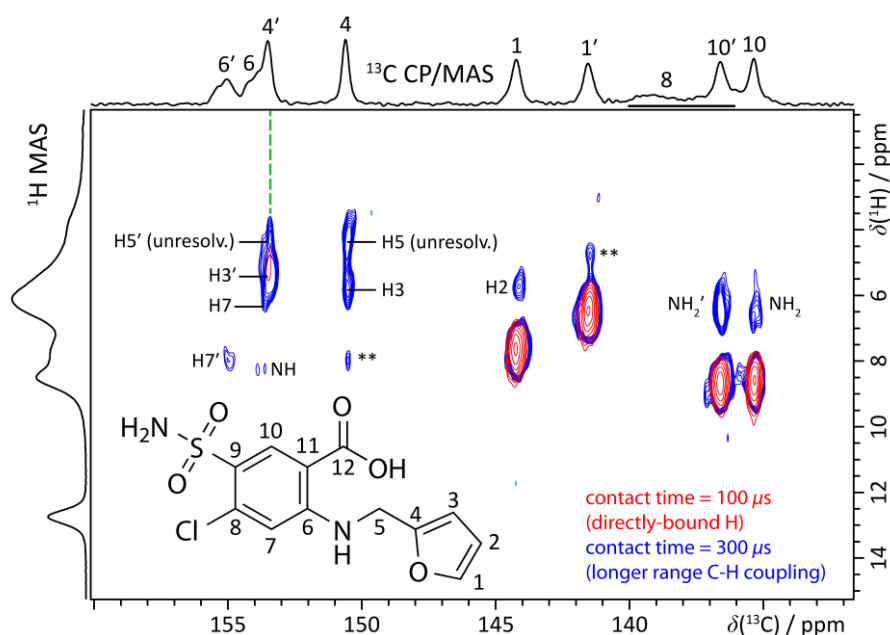


Figure S8. Partial expanded view of ^1H - ^{13}C refocused dipolar FSLG-HETCOR NMR spectra ($B_0 = 11.7\text{ T}$, contact time = $100\ \mu\text{s}$, red; contact time = $300\ \mu\text{s}$, blue) with site assignments for the furoseamide molecule (inset, **S-A** sample). The top horizontal axis shows the ^{13}C CP/MAS NMR spectrum, while the left vertical axis is the ^1H fast MAS NMR spectrum of the same material. Double asterisks indicate low intensity signals that did not appear in additional HETCOR experiments. The large bar under site 8 (the C-Cl carbon) denotes the anticipated linewidth (calculated with WSolid1⁵) of this site due to RDC to $^{35/37}\text{Cl}$.

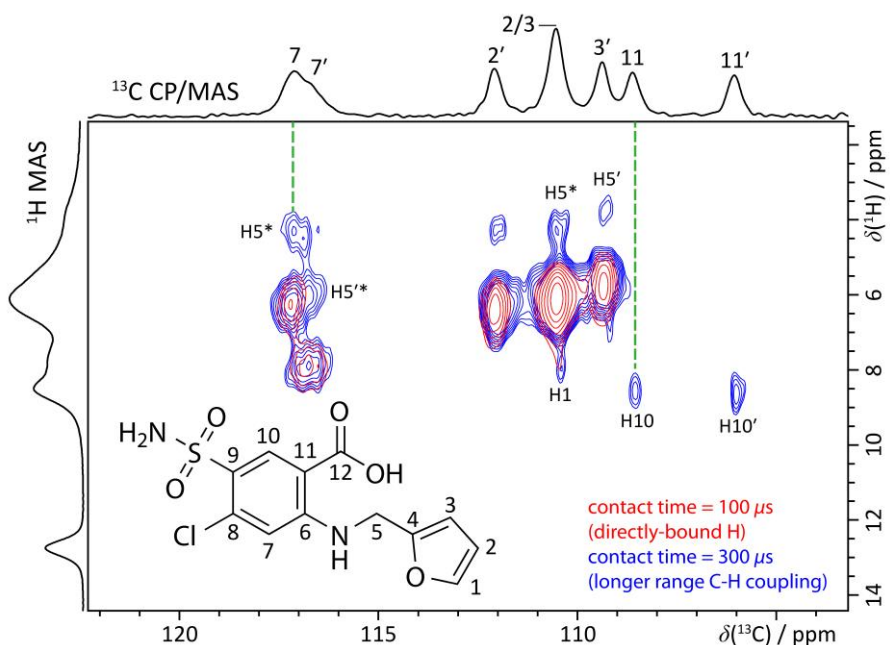


Figure S9. Partial expanded view of ^1H - ^{13}C refocused dipolar FSLG-HETCOR NMR spectra ($B_0 = 11.7\text{ T}$, contact time = $100\ \mu\text{s}$, red; contact time = $300\ \mu\text{s}$, blue) with site assignments for the furoseamide molecule (inset, **S-A** sample). The top horizontal axis shows the ^{13}C CP/MAS NMR spectrum, while the left vertical axis corresponds to the ^1H fast MAS NMR spectrum of the same material.

Table S5. Computational details and computed system enthalpies^a

structure	calculation type	plane wave cut-off energy / eV	enthalpy / eV
FURSEM01	H optimisation	520	-22181.131
	all atom optimisation	520	-22182.158
	not optimised, NMR calculation	800	-22181.324
	H-optimised, NMR calculation	800	-22186.495
	all-optimised, NMR calculation	800	-22187.515
FURSEM17	H optimisation	520	-22178.927
	all atom optimisation	520	-22181.097
	not optimised, NMR calculation	800	-22160.252
	H-optimised, NMR calculation	800	-22184.299
	all-optimised, NMR calculation	800	-22186.467
FURSEM-NEW	H optimisation	520	-22181.664
	all atom optimisation	520	-22182.183
	not optimised, NMR calculation	800	-22158.171
	H-optimised, NMR calculation	800	-22187.035
	all-optimised, NMR calculation	800	-22187.546

^a Quantum chemical computations were carried out using the Cambridge Serial Total Energy Package (CASTEP),⁶ version 8.0, using the default ultrasoft pseudopotentials to describe core electron states. Valence electron states were described via a plane wave basis set with energy cut-offs of 520 eV for geometry optimisations and 800 eV for NMR parameter calculations. Sampling of the Brillouin zone was done using a Monkhorst-Pack grid⁷ in k -space with a spacing of 0.05 \AA^{-1} , which corresponded to a $3 \times 3 \times 2$ k -point grid for all furosemide systems. In all cases, the generalized gradient approximation exchange-correlation functional of Perdew, Burke, and Ernzerhof (PBE)^{8,9} was used. NMR parameter calculations required the use of the gauge-including projector augmented-wave (GIPAW) method.^{10,11} When performing unit cell optimisations (as part of the dc-DFT protocol described in the main paper), dispersion-corrections according to Tkatchenko and Scheffler were used.¹² Atomic root-mean-squared difference values were established using the crystal packing similarity tool in Mercury (version 3.5.1).

Table S6. GIPAW DFT-computed magnetic shielding values for various furosemide crystal structures^a

label ^b	FURSEM01 (no opt)	FURSEM01 (H-opt)	FURSEM01 (all-opt)	FURSEM17 (no opt)	FURSEM17 (H-opt)	FURSEM17 (all-opt)	FURSEM-NEW (no opt)	FURSEM-NEW (H-opt)	FURSEM-NEW (all-opt)
C1	31.6660	33.5151	24.7844	33.7501	33.0549	25.4249	29.1487	27.7321	24.3018
C2	64.3391	69.3973	59.8801	67.0329	68.1386	59.8627	70.9824	65.8670	60.1117
C3	64.3975	65.9902	57.8518	72.7593	68.1822	56.8149	69.0287	62.3722	57.4308
C4	26.2357	25.7973	17.4954	27.0809	27.5720	17.5381	18.2819	21.1584	17.6644
C5	132.6120	133.4203	133.3951	149.0089	133.9946	132.7878	146.2637	132.9393	133.3285
C6	21.5836	20.4086	19.2340	23.7756	21.0865	18.6605	22.6988	19.9185	19.2235
C7	53.7597	54.7382	53.1556	59.6518	54.0308	53.1658	57.9313	52.0711	52.5797
C8	32.1923	30.0153	28.3859	34.8342	33.2137	29.5264	26.3817	28.6642	28.8069
C9	46.8509	43.7999	41.5806	47.3987	45.8179	41.6351	41.9996	43.3577	41.3523
C10	40.6807	38.3049	35.5140	45.0321	35.7673	38.1840	42.6877	37.0151	35.5216
C11	66.1864	64.3992	62.6786	62.6482	62.7086	61.6176	62.7524	64.1312	62.0652
C12	0.2862	-0.1436	-3.7827	6.8333	3.6198	0.5105	0.8571	-1.3264	-3.4250
C1'	32.7324	32.3821	27.4844	32.1072	32.1206	26.5625	31.4566	30.2527	27.6791
C2'	56.4136	62.7742	58.0927	62.8731	63.7952	57.5604	71.1278	62.7920	57.3493
C3'	61.7902	64.2059	59.9378	72.5628	67.3766	58.1967	71.1403	64.7230	59.8033
C4'	19.8353	20.0556	14.8803	20.9369	23.4783	17.1025	14.3249	17.5408	14.8547
C5'	132.9152	132.8759	132.9743	150.136	134.4085	132.1935	147.2579	133.0714	132.8786
C6'	19.6832	19.1278	18.0992	22.0385	20.3440	18.6935	18.4459	18.8320	18.2336
C7'	53.9590	54.0069	53.9140	57.6723	51.2238	55.1170	58.3843	53.6736	53.8840
C8'	30.9309	29.2140	27.8861	29.5927	26.4673	26.0918	29.5121	28.3913	28.2904
C9'	48.8423	46.4228	43.5039	48.7295	45.5725	44.3384	45.3247	45.6244	43.6940
C10'	38.0048	36.4402	33.9826	48.7538	39.3967	34.3174	39.8863	34.1857	33.9609
C11'	69.4676	67.2858	64.9573	67.4355	68.7438	64.3256	62.8136	65.2053	64.7616
C12'	0.9076	-0.0308	-3.4954	6.2585	1.6245	-2.3122	1.2294	-1.2383	-3.0943
C1-H	22.2131	22.8802	22.3448	24.5807	22.8191	22.5498	25.2520	22.3497	22.1609
C2-H	24.1767	24.6030	24.0861	26.4138	24.5890	24.0288	27.3657	24.3116	24.0254
C3-H	24.2773	24.7170	24.2548	27.1641	24.7839	24.2805	27.8119	24.4265	24.1429
C5-H	26.0736	25.8546	25.5007	30.0169	25.8985	25.7408	29.1692	25.8453	25.7703
C5-H*	26.4299	26.6520	26.5172	30.5480	26.7102	26.6840	30.0227	26.6170	26.5479
NH	20.8872	21.6471	21.5751	27.0008	20.8919	20.5830	28.7093	21.7785	21.6770
C7-H	24.7147	25.1384	25.1391	27.4169	25.0935	25.2042	27.2697	25.0657	25.1214
C10-H	22.3712	22.2035	22.0994	24.6481	22.1560	22.2662	24.1653	22.2107	22.1132
C12-OOH	14.5920	16.4145	15.6378	23.8058	17.6431	19.8583	21.1381	16.8736	16.1683
NH ₂	20.9292	23.6383	23.0893	28.3016	23.6905	24.4154	31.1282	23.8585	23.2979
NH ₂ *	22.6773	23.2905	22.6757	29.7299	23.3889	24.7800	30.5820	23.0300	22.5253
C1-H'	23.4423	23.9603	23.6642	25.6013	24.0102	23.6851	26.4901	23.8619	23.6382
C2-H'	23.4296	24.0415	23.7470	26.0154	24.0191	23.5434	27.2382	23.8355	23.5265
C3-H'	24.7452	25.1265	25.0256	27.6486	25.2132	24.9155	28.5268	25.1473	24.9275
C5-H'	26.4393	26.4234	26.2758	30.2023	26.3977	25.9397	29.4060	26.4722	26.4187
C5-H**	25.4867	25.4099	25.3565	29.4237	25.3466	25.0055	28.9336	25.4201	25.3159
NH'	20.3862	21.9395	22.1156	27.2725	22.1068	22.9363	28.6441	22.1856	22.2124
C7-H'	22.6569	22.9404	22.7966	25.3589	22.7195	23.3251	25.0701	22.7893	22.7341
C10-H'	22.1470	22.1242	21.9493	24.9867	22.3694	21.9638	23.8529	22.0568	22.0142
C12-OOH'	14.1031	16.6294	15.8308	25.1432	21.7826	21.6159	21.4801	17.2932	16.4195
NH ₂ '	21.0299	24.6316	24.1954	28.4352	24.4985	24.3230	31.5142	24.8766	24.5264
NH ₂ *'	23.1783	23.2675	23.0834	29.9229	23.2578	24.1873	30.5722	22.9666	22.5876
NH	117.1753	131.9954	129.5462	152.9052	136.8641	134.9159	152.1233	129.7947	128.4875
NH ₂	130.9399	142.1497	135.2045	176.2438	145.5323	132.2277	173.7718	142.2848	134.4364
NH'	108.0183	121.8118	121.8568	142.3318	122.7292	122.1651	145.1931	123.0618	121.7121
NH ₂ '	133.7800	142.3981	135.3011	169.8702	143.3555	136.7910	170.1887	142.2629	135.3163

^a Column headings 'no opt', 'H-opt' and 'all-opt' refer to cases where: no structural optimisation was done prior to magnetic shielding calculations; where the H atoms only were allowed to relax prior to magnetic shielding calculations; and where all atoms were allowed to relax prior to magnetic shielding calculations, respectively. Unit cell dimensions were fixed in all above cases.

^b See Scheme S1 for the distinction between the two molecules in the asymmetric unit, and specifications for the C5-H and NH₂ hydrogen atoms.

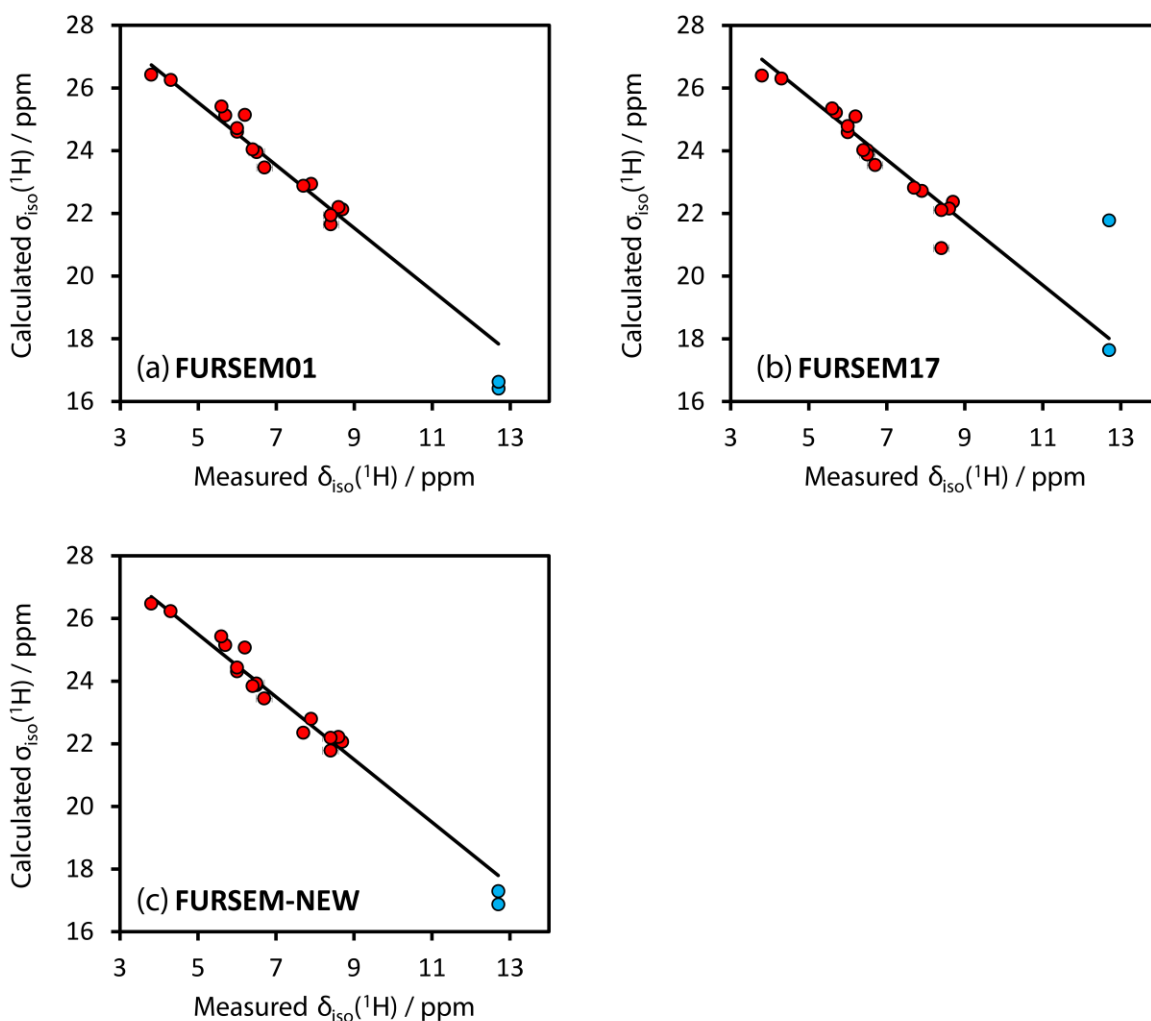


Figure S10. Correlation plots relating computed ^1H isotropic magnetic shielding values with each of the resolved experimental isotropic chemical shift values for H-optimised structures of **FURSEM01** (a), **FURSEM17** (b), and **FURSEM-NEW** (c). Data points coloured in light blue indicate the carboxyl hydrogen atoms. As can be clearly seen, the structure of **FURSEM17** leads to calculated magnetic shielding values for these sites that are very much different (over 4 ppm apart), contrary to ^1H measurements on **S-A** and **ReCryst** samples of furosemide, and also at odds with those calculated using the **FURSEM01** and **FURSEM-NEW** structures. Lines of best linear fit (gradient fixed at -1) are as follows: (a) $\sigma_{\text{iso}}(^1\text{H}) = -\delta_{\text{iso}}(^1\text{H}) + 30.537$ ppm; (b) $\sigma_{\text{iso}}(^1\text{H}) = -\delta_{\text{iso}}(^1\text{H}) + 30.717$ ppm; (c) $\sigma_{\text{iso}}(^1\text{H}) = -\delta_{\text{iso}}(^1\text{H}) + 30.496$ ppm.

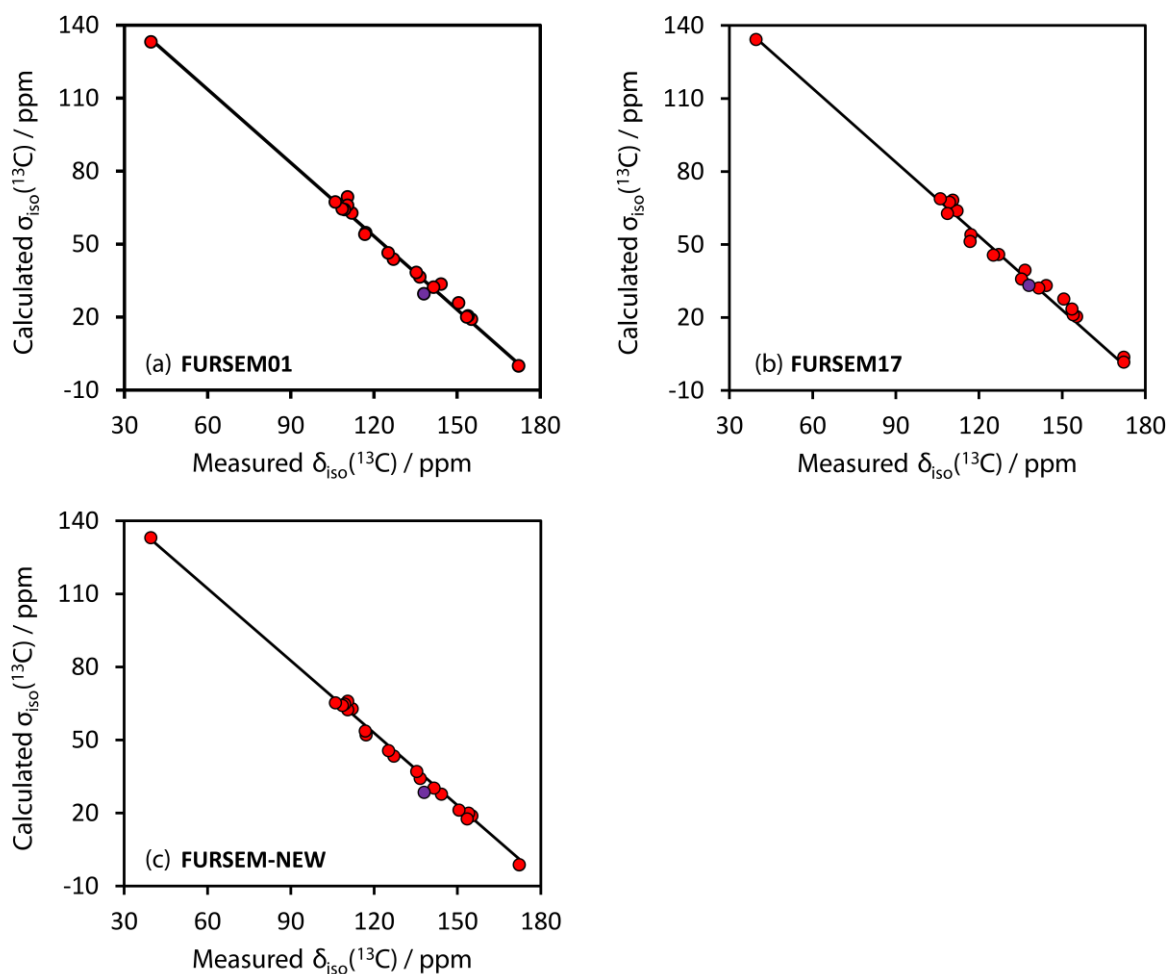


Figure S11. Correlation plots relating computed ^{13}C isotropic magnetic shielding values with each of the resolved experimental isotropic chemical shift values for H-optimised structures of **FURSEM01** (a), **FURSEM17** (b), and **FURSEM-NEW** (c). Data points coloured in purple indicate the carbon in the C-Cl bond, which was not included in the fitting process due to the imprecise measurement of this chemical shift. Lines of best linear fit are as follows: (a) $\sigma_{\text{iso}}(^{13}\text{C}) = -1.0055\delta_{\text{iso}}(^{13}\text{C}) + 173.94$ ppm; (b) $\sigma_{\text{iso}}(^{13}\text{C}) = -1.0123\delta_{\text{iso}}(^{13}\text{C}) + 174.94$ ppm; (c) $\sigma_{\text{iso}}(^{13}\text{C}) = -0.9895\delta_{\text{iso}}(^{13}\text{C}) + 171.62$ ppm.

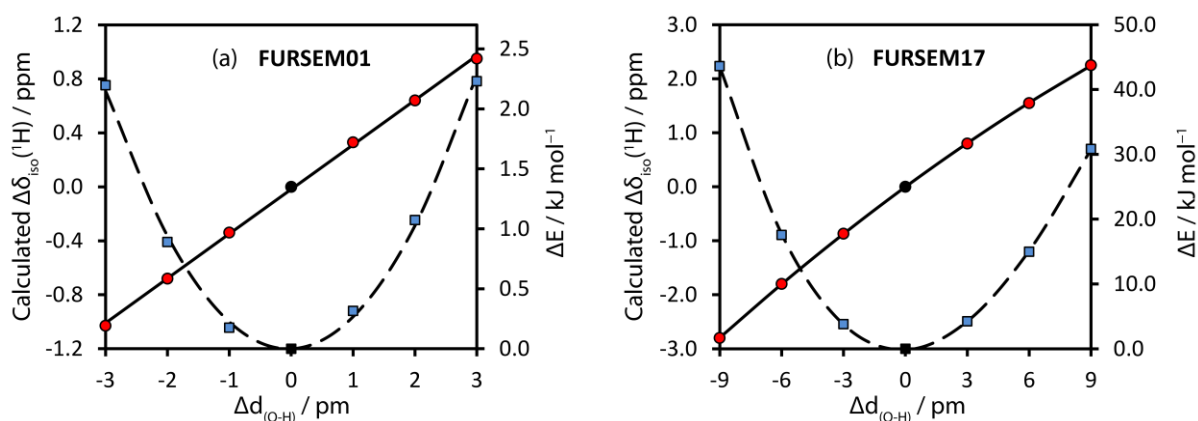


Figure S12. Correlation plots relating computed ^1H isotropic chemical shift value changes (circles) and lattice enthalpy changes (squares) using the H-optimised structures of **FURSEM01** (a), and **FURSEM17** (b) as references (reference data points are indicated in solid black) as a function of OH internuclear distance variation. Concretely, we varied the position of the C12-OOH' hydrogen atom, (label is as specified in Table S6). Lines of best fit are as follows: (a) $\Delta\delta_{\text{iso}}(^1\text{H}) / \text{ppm} = 0.3304\Delta d_{(\text{O-H})} / \text{pm} - 0.0186$; $\Delta E / \text{kJ mol}^{-1} = 0.2459\Delta d_{(\text{O-H})}^2 / \text{pm}^2 + 0.0217\Delta d_{(\text{O-H})} / \text{pm} - 0.0012$; (b) $\Delta\delta_{\text{iso}}(^1\text{H}) = -0.00336\Delta d_{(\text{O-H})}^2 / \text{pm}^2 + 0.280\Delta d_{(\text{O-H})} / \text{pm} - 0.0033$; $\Delta E / \text{kJ mol}^{-1} = -0.0109\Delta d_{(\text{O-H})}^3 / \text{pm}^3 + 0.4604\Delta d_{(\text{O-H})}^2 / \text{pm}^2 + 0.1763\Delta d_{(\text{O-H})} / \text{pm} - 0.1472$. Hence, in **FURSEM01**, the OH distance would need to be changed by a trivial amount of ca. -0.03 \AA to minimize the RMSD contribution for this site. This comes with an associated lattice enthalpy cost of $2 - 3 \text{ kJ mol}^{-1}$. Conversely, we would need to change the OH distance in **FURSEM17** by ca. $+0.13 \text{ \AA}$ (arrived at by extrapolation) to achieve the same RMSD minimization, which is a meaningful structural change. Importantly, this structural change comes with an enthalpy cost of nearly 100 kJ mol^{-1} , which would not be accessible.

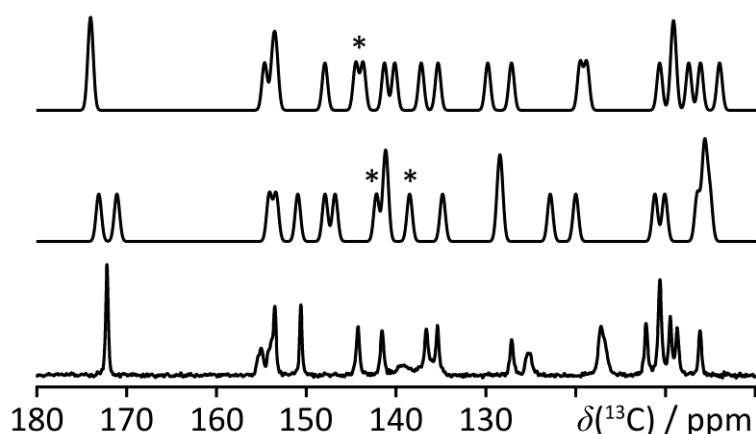


Figure S13. Comparison between calculated and experimental ^{13}C NMR spectra (omitting the C5/C5' signals), using the data in Table S6 and Figure S11, with Gaussian line broadening. From the top, the traces correspond to **FURSEM01**, **FURSEM17** and **S-A** (experimental), respectively. The peaks indicated by the asterisks correspond to the C-Cl carbons, which were omitted from the RMSD calculation.

Table S7. ^1H RMSD calculation for **FURSEM-NEW** (H-opt)^a

label	δ_{iso} / ppm (experiment)	σ_{iso} / ppm (GIPAW DFT)	δ_{iso} / ppm (regression)	$w\chi^2(\delta_{\text{iso}})$ / ppm ²	weight ^b
OH	12.7	16.8736	13.623	0.4257	0.5
OH'	12.7	17.2932	13.203	0.1266	0.5
10'	8.7	22.0568	8.439	0.0679	1
10	8.6	22.2107	8.286	0.0989	1
NH	8.4	21.7785	8.718	0.0505	0.5
NH'	8.4	22.1856	8.311	0.0040	0.5
7'	7.9	22.7893	7.707	0.0373	1
1	7.7	22.3497	8.147	0.1994	1
NH ₂ ,avg	6.7	23.4443	7.052	0.1239	1
1'	6.5	23.8619	6.634	0.0181	1
NH ₂ ' ₁ ,avg	6.5	23.9216	6.575	0.0056	1
2'	6.4	23.8355	6.661	0.0680	1
7	6.2	25.0657	5.431	0.5920	1
2	6.0	24.3116	6.185	0.0171	0.5
3	6.0	24.4265	6.070	0.0024	0.5
3'	5.7	25.1473	5.349	0.1232	1
5*'	5.6	25.4201	5.076	0.2744	1
5,avg	4.3	26.2312	4.265	0.0012	1
5'	3.8	26.4722	4.024	0.0502	1
			SUM, $w\chi^2$	2.286	ppm ²
			RMSD	0.378	ppm
Summary					
<i>b</i>	30.496	ppm			
<i>m</i>	-1				
RMSD	0.378	ppm			

^a All RMSD calculations were performed using the 'solver' module contained within Microsoft Excel 2010, *via* a minimisation of the sum of the weighted difference squared values ($w\chi^2$) under the fit function $\sigma_{\text{iso}} = m\delta_{\text{iso}} + b$. For ^1H RMSD calculations, *m* was restrained to -1 , while it was allowed to freely vary in the ^{13}C RMSD calculations reported in the main manuscript. ^{13}C RMSD calculations were also attempted using a fixed *m* of -1 , but did not yield ^{13}C RMSD that were significantly different. All other RMSD calculations for ^1H and ^{13}C were conducted in an analogous manner.

^b Weighting was such that each experimentally resolved peak was assigned a weighting of unity.

References

- (1) Babu, N. J.; Cherukuvada, S.; Thakuria, R.; Nangia, A. *Cryst. Growth Des.* **2010**, *10*, 1979.
- (2) Dolomanov, O. V.; Bourhis, L. J.; Gildea, R. J.; Howard, J. A. K.; Puschmann, H. *J. Appl. Cryst.* **2009**, *42*, 339.
- (3) Sheldrick, G. M. *Acta Cryst. A* **2008**, *A64*, 112.
- (4) Thurber, K. R.; Tycko, R. *J. Magn. Reson.* **2009**, *196*, 84.
- (5) Eichele, K.; Wasylishen, R. E. *WSolids NMR Simulation Package*, v. 1.20.22, **2014**.
- (6) Clark, S. J.; Segall, M. D.; Pickard, C. J.; Hasnip, P. J.; Probert, M. I. J.; Refson, K.; Payne, M. C. *Z. Kristallogr.* **2005**, *220*, 567.
- (7) Monkhorst, H. J.; Pack, J. D. *Phys. Rev. B* **1976**, *13*, 5188.
- (8) Perdew, J. P.; Burke, K.; Ernzerhof, M. *Phys. Rev. Lett.* **1996**, *77*, 3865.
- (9) Perdew, J. P.; Burke, K.; Ernzerhof, M. *Phys. Rev. Lett.* **1997**, *78*, 1396.
- (10) Pickard, C. J.; Mauri, F. *Phys. Rev. B* **2001**, *63*, 245101.
- (11) Yates, J. R.; Pickard, C. J.; Mauri, F. *Phys. Rev. B* **2007**, *76*, 024401.
- (12) Tkatchenko, A.; Scheffler, M. *Phys. Rev. Lett.* **2009**, *102*, 073005.